^{95}Mo(n,α) cross section from 1 eV to 500 keV: A test of the α+nucleus optical potential used in calculating reaction rates for explosive nucleosynthesis

W. Rapp,[1,2,*] P. E. Koehler,[1] F. Käppeler,[2] and S. Raman[1,†]
[1]*Physics Division, MS-6354 Oak Ridge National Laboratory, Oak Ridge, Tennessee 37831, USA*
[2]*Forschungszentrum Karlsruhe, Institut für Kernphysik, Postfach 3640, D-76021 Karlsruhe, Germany*
(Received 31 January 2003; published 29 July 2003)

We have measured the ^{95}Mo(n,α) cross section in the energy range from 1 eV to 500 keV at the Oak Ridge Electron Linear Accelerator (ORELA). This work is part of a series of (n,α) measurements for deriving a reliable global α+nucleus potential, which is an essential ingredient in nuclear statistical model calculations of the reaction rates for unstable nuclei involved in explosive *p*-process nucleosynthesis. The ^{95}Mo(n,α) rate shows a strong sensitivity to the α+nucleus potential used in the calculations, and therefore these new data should be very useful in obtaining an improved potential. For example, although there is a factor of 5 variation in the rate calculated using different potentials, an older model and a newer one using one of three recently proposed potentials are in good agreement with our new data.

DOI: 10.1103/PhysRevC.68.015802 PACS number(s): 26.30.+k, 27.60.+j

I. INTRODUCTION

Over the last decade explosive nucleosynthesis has become a subject of increasingly quantitative analyses. One of the scenarios which has been studied in this context is the so-called *p* process, which is the name given to the mechanism through which the neutron deficient isotopes of intermediate- to heavy-mass elements are formed. In the leading model of the *p* process, the shock front from type II supernova explosions ignites explosive burning in oxygen/neon layers on a time scale of about 1 s and at temperatures between 2 and 3×10^9 degrees. Under these conditions, the *p* nuclides are synthesized by photodisintegration reactions on *s*- and *r*-process seed nuclides (for more details see Ref. [1]). The seed nuclides are shifted by (γ,n) reactions to the point where (γ,n) and (n,γ) reactions are in equilibrium. Then the reaction flow can proceed further only by (γ,α) and (γ,p) reactions. Hence (γ,α) reaction rates across a broad mass range play an important role in the extended network calculations that are required to describe the final *p*-process abundances [2,3].

Determination of (γ,α) rates at astrophysically relevant temperatures via direct measurements [or via inverse (α,γ) measurements] is exceedingly difficult because the corresponding energies are well below the Coulomb barrier so that the cross sections are extremely small. Therefore, very few measurements have been reported so far. On the other hand, these rates should be calculable to sufficient accuracy using the nuclear statistical model. However, statistical model calculations are hampered by the uncertain α+nucleus optical potential in the astrophysically relevant energy range. The α+nucleus optical potential is needed to calculate the transmission probability of the α particle through the Coulomb barrier of the nucleus and, therefore, has a large impact on the calculated rates. The potentials are thought to depend on several parameters related to the properties of the target nuclides, so it is important to have data across as wide a range of the parameter space as possible. It recently has been shown [4] that a series of (n,α) measurements may offer the best opportunity for enabling the needed global improvements in the α+nucleus potential for astrophysics applications.

Principally, (n,α) cross section measurements provide a twofold advantage over other techniques: (i) *Q* values for (n,α) reactions correspond well with the astrophysically relevant range of the *p* process, so that extrapolations inherent in other approaches [5] are not necessary. The very few (α,γ) data that exist demonstrate the large uncertainties associated with such extrapolations. (ii) Through scaling from previous measurements using predicted cross sections, (n,α) measurements for about 30 intermediate- to heavy-mass nuclides should be possible. Therefore, this set of measurements should lead to the needed global improvement in the calculations. In addition, it has been shown that (n,α) cross-section measurements can be very useful in constraining the α potential used in the statistical model. For example, in Ref. [6] it was shown that calculated (α,n) rates, via the α-transmission coefficients, are sensitive to the α potential used in the statistical model. Detailed balance arguments require that (n,α) rates show a similar sensitivity, and this was recently demonstrated [4] for the case of ^{147}Sm(n,α) in which different published α potentials resulted in a factor of 30 variation in the calculated reaction rates. Furthermore, recent α-induced cross section measurements for ^{96,98}Ru [7] as well as (n,α) measurements for ^{143}Nd [8] and ^{147}Sm [4] have shown that the commonly used statistical model code NON-SMOKER [9] systematically overestimates the reaction rates by factors of 2–3 and the similar code MOST [11] underestimates the (n,α) rates by approximately the same factors, but the older calculations of Holmes *et al.* [10] agree with the data to better than 30%. The present work extends the experimental data to the important region near the *p* nuclide ^{92}Mo that consistently has been underproduced in almost all *p*-process calculations.

*Electronic address: wolfgang.rapp@ik.fzk.de
†Deceased.

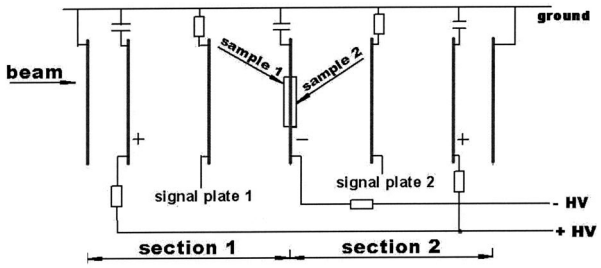

FIG. 1. Schematic sketch of a compensated ionization chamber for (n,α) cross-section measurements.

II. EXPERIMENTAL SETUP

The ^{95}Mo(n,α) cross section was measured at the ORELA white neutron source. The ORELA linear accelerator was used to generate a pulsed beam of 150 MeV electrons at a repetition rate of 525 Hz and a pulse width of 8 ns. Neutrons were produced via (γ,n) reactions from the intense bremsstrahlung photon flux generated as electrons slowed down in a Ta target. The neutron energy was determined by the time of flight (TOF) method. The shortest possible flight path was used to obtain the maximum flux because the investigated cross section is very small.

The samples consisted of two metallic ^{95}Mo (96.8%-enriched) foils that were 5 mg/cm^2 thick by 11 cm in diameter each. The samples were placed back to back on either side of a thin Al foil and were oriented perpendicular to the well-collimated (10-cm-diameter) neutron beam in the center of a compensated ionization chamber (CIC) at a distance of 8.840 m from the neutron source. This geometry enabled measurement of the ^{95}Mo(n,α) cross section independent of the angular distribution of the emitted α particles. A second small CIC containing a thin ^{6}LiF sample was installed 1.2 m downstream of the ^{95}Mo sample and served as a flux monitor.

The intense γ flash at the start of each neutron pulse was reduced by a 5-mm-thick Pb filter placed in the beam line at a distance of 5 m from the neutron source. In addition, a 0.3-mm-thick Cd filter was used at this position to eliminate the overlap of slow neutrons from previous pulses. Effects due to the γ flash have limited previous (n,α) cross-section measurements made with ordinary ion chambers to energies below a few keV [12]. However, in the present experiment the range could be extended to 500 keV by using a CIC as the detector.

The principle of such a detector is described in Ref. [13] and is illustrated in Fig. 1. The signal plate is sandwiched between two electrodes having high voltages equal in magnitude, but opposite in sign. In this way, the ionization effect due to the γ flash is equal in the volumes on both sides of the central plate, but induces signals of opposite polarity on this plate so that the residual signal due to the γ flash is nearly zero. In contrast, the α particles emitted from the sample interact with the counting gas only on one side of the signal plates, thus producing measurable net signals. The counting gas consisted of argon with an admixture of 10% CO_2 to enhance the electron drift velocity [14,15]. The high voltage applied to the sample plate was -3000 V. The corresponding positive voltage was adjusted experimentally for optimal suppression of the γ flash.

Monte Carlo simulations were performed with the TRIM code [16] to calculate the path length of the α particles. At a pressure of 1.2 bar, the 42.4-mm path length of the 6.5-MeV α particles was always smaller than the distance from the sample to the signal plate of 45.7 mm. Hence the stopping point of the α particles is far enough from the signal plates to separate the fast-moving electrons from the ions and to obtain an explicit signal.

III. MEASUREMENT

A first measurement was carried out for determining the neutron flux at the location of the ^{95}Mo sample. For this purpose, the main CIC contained a ^{6}LiF sample in the upstream position and a ^{95}Mo sample in the downstream position. The run with this configuration lasted for 32 h.

In subsequent runs, the ^{6}LiF sample in the main CIC was replaced by a second ^{95}Mo sample. A total of 540 h of beam time was run in this configuration. The monitor CIC remained in a single position during the entire experiment and was used to normalize the relative flux between these two sets of runs.

IV. DATA ANALYSIS

The TOF (1 ns/channel resolution) and pulse height of each α particle detected in both the main and monitor CICs were recorded in event mode and used to generate two-dimensional spectra. For ^{95}Mo$(n,\alpha)^{92}$Zr, a pulse-height threshold of 2 MeV was used to eliminate low-energy background signals. The recorded data were evaluated in the following steps.

(i) Counting loss corrections (to account for the 25 μs dead time associated with each event) were calculated using standard techniques and applied on a channel-by-channel basis. The average dead time correction was less than 2.5%, but was as high as 12% at neutron energies near the peak of the 250-keV ^{6}Li resonance during the measurement with the ^{6}LiF sample inside the main CIC.

(ii) The time-independent background was determined at the low end of the energy range where all neutrons had been absorbed by the Cd filter and subtracted.

(iii) The data were corrected using the code SRIM [16] for α straggling in the samples and imperfect charge collection causing α-particle signals to occur below threshold.

Because our samples were relatively thick and because the inherent resolution of a CIC is rather poor, we could not resolve the various α-particle groups emitted to the ground and excited states of ^{92}Zr. However, because the α particles are emitted at energies below the Coulomb barrier, the penetrability—and hence the cross section—is a steep function of the emitted α-particle energy. Therefore, all transitions except for those to the ground state ($E_\alpha = 6.123$ MeV) and the first excited state ($E_\alpha = 5.227$ MeV) are strongly suppressed and, according to penetrability calculations that we have made, are expected to account for less than 2% of the cross section. Therefore, only these two

groups were taken into consideration when calculating this correction. The simulated α particles were started with uniformly distributed random positions and emission angles in the sample. Pulse-height spectra were constructed from the calculated α-particle ranges using an approximation [17] for the pulse height H,

$$H = 1 - \frac{3}{5}\frac{R_0}{d}\cos(\theta) \tag{1}$$

where R_0 denotes the range of the α particles, d the 45.7-mm distance between the plates, and θ the angle between the direction of the α particles and the neutron beam. The stopping power in the counting gas was calculated using SRIM for a pressure of 1.2 bar as a function of the α-particle energy. The results were fitted with a second-degree polynomial,

$$R_0 = 0.8855 + 2.9022E_\alpha + 0.5313E_\alpha^2, \tag{2}$$

with the α energy E_α in MeV and the range R_0 in mm. From these spectra, the correction factor for absorption losses and for effect of the electronic threshold was determined to be $K_{\rm abs} = 1.20 \pm 0.02$. The corresponding correction for the ^{6}LiF sample used in the first run was negligible because it was only $(1.19 \pm 0.02) \times 10^{10}$ atoms/cm^2 in thickness.

(iv) The cross section was eventually evaluated via

$$\sigma = 2K_{\rm abs}\frac{n_{\rm Li}}{n_{\rm Mo}}\frac{R_{{\rm Li},M}}{R_{{\rm Mo},M}}\frac{R_{\rm Mo}}{R_{\rm Li}}\sigma_{\rm Li}, \tag{3}$$

where the factor of 2 accounts for the fact that both the α and ^{3}H particles were detected from each ^{6}Li$(n,\alpha)^3$H reaction in the main CIC during the calibration run. The factor $K_{\rm abs} = 1.20 \pm 0.02$ corrects for absorption losses as described above, and $n_{\rm Li}$ and $n_{\rm Mo}$ denote the number of ^{6}Li [$(1.19 \pm 0.02) \times 10^{-6}$ atom/barn] and ^{95}Mo [$(6.138 \pm 0.025) \times 10^{-5}$ atom/barn] atoms in the samples, respectively. $R_{{\rm Li},M}$ corresponds to the counts from the ^{6}Li$(n,\alpha)^3$H reaction in the monitor CIC during the calibration run and $R_{{\rm Mo},M}$ to the counts from this reaction in the same energy range in the monitor CIC during the ^{95}Mo measurement. $R_{\rm Mo}$ corresponds to the ^{95}Mo(n,α) counts per channel during the ^{95}Mo measurement and $R_{\rm Li}$ to the ^{6}Li$(n,\alpha)^3$H counts per channel in the main CIC during the calibration run. Finally, $\sigma_{\rm Li}$ corresponds to the well-known ^{6}Li(n,α) cross section [18].

TABLE I. Experimental uncertainties.

Quantity	Uncertainty (%)
Mo sample	± 0.4
^{6}Li sample	± 2.5
$\sigma_{\rm Li}$	± 2.0
$R_{{\rm Li},M}/R_{{\rm Mo},M}$	± 0.2
$K_{\rm abs}$	± 2.0
Statistics	$\pm$(2.7–16.2)

The data used in the $\mathcal{R}$-matrix analysis were averaged over several TOF channels between resonances to improve the statistical precision. To compare to statistical model calculations, the data were averaged into 12 energy bins between 1 and 500 keV. The respective uncertainties are listed in Table I. The overall uncertainty was determined by assuming that all uncertainties are independent of each other.

V. RESONANCE ANALYSIS

The data were fitted with the $\mathcal{R}$-matrix code SAMMY [19] to extract resonance areas and α widths for resonances in the resolved region below 2.2 keV. Representative plots of the data and $\mathcal{R}$-matrix fits are shown in Fig. 2. The resulting

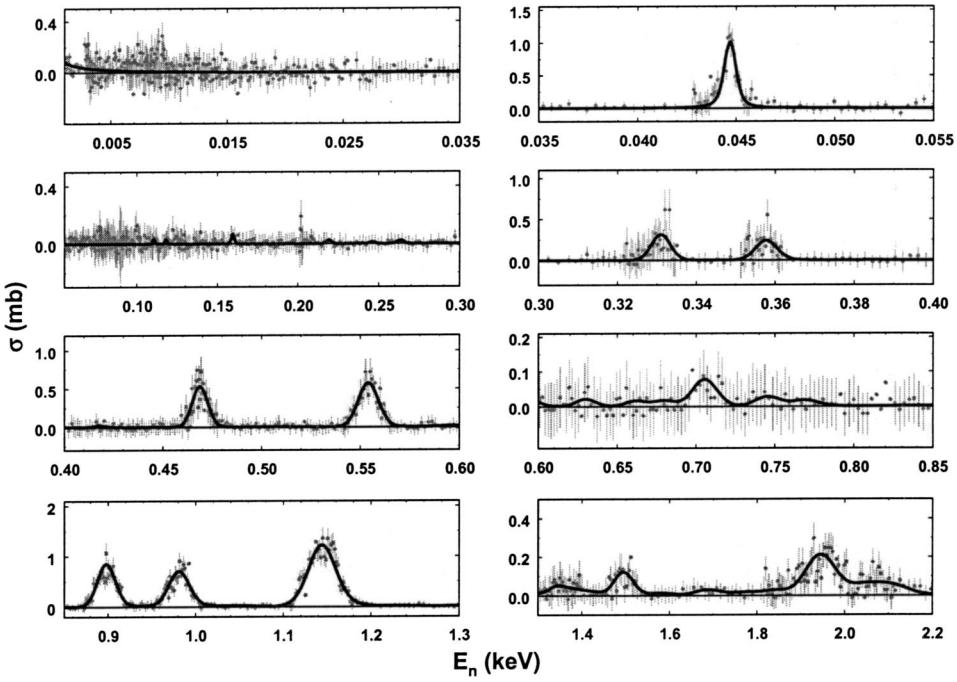

FIG. 2. ^{95}Mo(n,α) cross-section data (points with error bars) and SAMMY fits (solid curves).

TABLE II. ^{95}Mo(n,α) resonance parameters.

E_n (eV)	J^π	$2g_J\Gamma_n$ (meV)	Γ_γ (meV)	Γ_α (μeV)	$g_J\Gamma_\alpha\Gamma_n/\Gamma$ (μeV)
−9.90	2^+	2.72	160	12.3 (*12*)	-
44.69	3^+	200 (*10*)	150 (*10*)	0.0349 (*21*)	0.0108 (*10*)
110.5	1^-	0.16 (*2*)	310 (*80*)	<11	<0.0028
117.8	$2^{(-)}$	0.15 (*2*)	200 (*120*)	<7.9	<0.0030
159.49	3^+	15 (*1*)	166 (*20*)	<0.24	<0.010
218.28	$(4)^-$	1.3 (*1*)	160	<2.4	<0.0097
245.84	(2^+)	0.50 (*5*)	160	<3.9	<0.0061
263.59	(3^+)	1.4 (*2*)	160	<3.1	<0.013
330.92	$(3)^-$	3.4 (5)	160	14.6 (*30*)	0.152 (*32*)
357.75	3^+	320 (*60*)	145 (*20*)	0.382 (*84*)	0.146 (*32*)
418.2	(2^+)	1.00 (*14*)	160	<13	<0.040
468.68	$(2)^-$	11 (*1*)	160	18.8 (*17*)	0.597 (*55*)
554.08	2^+	110 (*20*)	160	5.26 (*41*)	0.990 (*78*)
595.67	(3^+)	0.84 (*20*)	160	<16	<0.041
630.01	$(4)^-$	20 (*3*)	160	<1.6	<0.092
661.78	3^+	18.0 (*15*)	160	<1.5	<0.079
680.19	3^+	830 (*50*)	145 (*15*)	<0.19	<0.094
702.62	(2^+)	2.9 (*3*)	160	14.6 (*99*)	0.130 (*88*)
708.25	(3^+)	13.4 (*8*)	160	3.4 (*24*)	0.132 (*92*)
745.46	$(3)^-$	5.5 (*20*)	160	<10	<0.17
769.83	3^+	28 (*3*)	160	<1.6	<0.12
898.27	2^+	265 (*30*)	175 (*20*)	18.0 (*10*)	4.84 (*24*)
932.13	(3^+)	3.5 (*3*)	160	<16	<0.18
956.50	(2^+)	1.5 (*7*)	160	<46	<0.21
981.23	2^+	37 (*6*)	160	54.5 (31)	4.92 (*28*)
1011.1	$(3)^-$	12.6 (*10*)	160	<3.8	<0.14
1023.8	3^+	110 (*20*)	160	<0.60	<0.13
1035.7	(3^+)	13.2 (*10*)	160	<4.0	<0.15
1059.2	(2^+)	9.2 (*8*)	160	<7.5	<0.20
1122.5	(3^+)	4.0 (*6*)	160	74 (*31*)	0.91 (*38*)
1144.6	2^+	250 (*50*)	160	45.2 (*23*)	12.29 (*62*)
1170.5	(3^+)	20.6 (*18*)	160	10.3 (*55*)	0.60 (*32*)
1203.4	3^+	131 (*9*)	160	<0.80	<0.19
1296.9	(3^+)	11 (*1*)	160	<6.7	<0.22
1340.7	(3^+)	88	160	3.3 (*18*)	0.63 (*34*)
1360.6	(3^+)	6.0 (*8*)	160	<28	<0.50
1386.7	(3^+)	11.6 (*10*)	160	11.5 (*76*)	0.39 (*26*)
1419.3	(3^+)	620 (*70*)	170 (*12*)	<0.97	<0.43
1437.0	(3^+)	15.6 (*14*)	160	<6.2	<0.28
1495.5	(5^+)	360	160	4.77 (*91*)	2.40 (*46*)
1570.0	(3^+)	12 (*1*)	160	<5.0	<0.18
1576.8	(3^+)	10.4 (*8*)	160	<3.7	<0.12
1589.5	(5^+)	215	160	<0.85	<0.33
1677.4	(3^+)	100 (*25*)	160	2.5 (*18*)	0.51 (*37*)
1704.1	(3^+)	42.8 (*64*)	160	4.0 (*32*)	0.44 (*34*)
1766.1	(5^+)	270	160	<1.4	<0.62
1788.0	(3^+)	62 (*10*)	160	<3.0	<0.42
1841.7	(3^+)	38.8 (*52*)	160	6.2 (*38*)	0.62 (*38*)
1853.3	(3^+)	6.4 (*8*)	160	13 (*10*)	0.26 (*20*)
1925.1	(3^+)	36.0 (*46*)	160	22 (*13*)	2.0 (*12*)

TABLE II. (*Continued.*)

E_n (eV)	J^π	$2g_J\Gamma_n$ (meV)	Γ_γ (meV)	Γ_α (μeV)	$g_J\Gamma_\alpha\Gamma_n/\Gamma$ (μeV)
1950.2	(3^+)	390 (*110*)	144 (*20*)	14.7 (*35*)	6.0 (*14*)
1961.3	(3^+)	27.6 (*28*)	160	<18	<1.3
2048.1	(3^+)	245 (*100*)	160	7.0 (*26*)	2.31 (*84*)
2112.2	(3^+)	60 (*8*)	160	14.9 (*64*)	2.11 (*91*)

parameters are given in Table II. The firm J^π values as well as those $2g_J\Gamma_n$ ($g_J=(2J+1)/[(2I+1)(2i+1)]$, where J, I, and i are the spins of the resonance, ^{95}Mo, and the neutron, respectively) and Γ_γ values having uncertainties in this table were taken from Refs. [20], [21] which are based on the work of Refs. [22–29]. The neutron width for the first (subthreshold) resonance in this table is the reduced width at 1 eV ($2g_J\Gamma_n^0$) and the notation 12.3 (*12*) stands for 12.3 ± 1.2, etc.

Orbital angular momenta up to and including d waves were included in the $\mathcal{R}$ matrix. A radius of 7.0 fm was used in all channels. The aluminum backing was included in the input files for SAMMY so that corrections could be applied for attenuation and multiple-scattering effects in the sample and its backing. The resonance energies, spins, parities, and neutron and γ widths from the compilation of Ref. [20] were used as starting values in the analysis. Only a few of the energies had to be adjusted. A radiation width equal to the average for ^{95}Mo resonances (160 meV [20,21]) was used for resonances without Γ_γ values in Ref. [20]. Also for these resonances, if no spin assignment was given in Ref. [20], then the J values listed in Table II were chosen so that the radiation width calculated from the resonance areas $A_\gamma=g_J\Gamma_\gamma\Gamma_n/\Gamma$ and neutron widths given in Ref. [20] would yield a radiation width as close as possible to 160 meV. For some of the resonances in Ref. [20], however, the A_γ and $g_J\Gamma_n$ values are incompatible ($g_J\Gamma_n \leqslant A_\gamma$) and it was not possible to use this approach, so the spins for these resonances are arbitrary. No neutron widths are given in Ref. [20] for four of the resonances in this energy range. The $2g\Gamma_n$ values listed in Table II for these cases were calculated from the resonance areas in Ref. [20] using $\Gamma_\gamma=160$ meV and the (arbitrary) spins given in Table II. The resulting neutron widths for these four resonances, while consistent with the resonance areas, are so large that they easily should have been determined in previous total cross section measurements. Therefore, the neutron widths as well as the resulting α widths should be considered upper limits for these four resonances.

The accuracy of the extracted α widths depends on the accuracy of the J^π, Γ_n, and Γ_γ assignments for the resonances because our measurement technique determines only the resonance areas $A_\alpha=g_J\Gamma_\alpha\Gamma_n/\Gamma$. The uncertainties in the resonance areas in Table II are the one-standard-deviation uncertainties determined in fitting the data. The α widths carry additional uncertainties due to uncertainties in the J, Γ_n, and Γ_γ values used to calculate the Γ_α values from the resonance areas. Unfortunately, these parameters and their associated uncertainties are not very well determined for many of the resonances, so it is not possible to calculate the additional uncertainty they add to the Γ_α values. For this reason, the uncertainties in the α widths given in Table II represent only the one-standard-deviation uncertainties determined in fitting the data.

For 30 of the 54 resonances in this region, SAMMY determined that the fitted resonance areas had relative uncertainties greater than 70%. In these cases we give only upper limits for the resonance areas in Table II equal to the fitted values plus the one-standard-deviation uncertainties determined by SAMMY. The upper limits on the α widths given in Table II for these cases were calculated from the upper limits on the resonance areas using the listed spins and neutron and radiation widths. The uncertainties in the spins and neutron and radiation widths were not taken into account when calculating these α-width upper limits.

The present results are a substantial improvement over previous work [12] in which only seven resonance areas were measured. However, because the spins and radiation widths for many of the resonances have not been determined, the Γ_α values given in Table II are of limited usefulness at present. If knowledge of these other resonance parameters is improved by future measurements, then the parameters in Table II could be used to calculate a more reliable set of α widths. This improved set could be very useful for improving the statistical model because it would eliminate the confounding influences of other model parameters and allow a more direct approach for improving the α+nucleus potential in the model. At present however, it is more useful to compare the statistical model calculations to the cross-section data.

VI. COMPARISON TO STATISTICAL MODEL CALCULATIONS

For a meaningful comparison to the statistical model, it is necessary to average over many resonances. The measured cross sections averaged over coarse bins are listed in Table III and compared in Fig. 3 to statistical model predictions. The calculated cross sections of Holmes *et al.* [10] and from the code MOST [30] using potential II are in good agreement with the present results, whereas the standard NON-SMOKER [9] values are larger than the data by a constant factor of 2.25 and the MOST calculations using potentials I and III are factors of 2.3 and 2.2 above and below the data, respectively.

The more recent NON-SMOKER and MOST models differ from the model used by Holmes *et al.* in the prediction of

TABLE III. ^{95}Mo(n,α) cross sections averaged over coarse bins.

Energy bin (keV)	$\sigma(n,\alpha)$ (μbarn)
1.5 ± 0.5	89.6 ± 4.4
2.5 ± 0.5	104.4 ± 5.1
3.5 ± 0.5	72.0 ± 4.9
4.5 ± 0.5	87.0 ± 5.8
6.25 ± 1.25	30.6 ± 3.5
8.75 ± 1.25	47.8 ± 3.8
12.5 ± 2.5	30.1 ± 2.6
20.0 ± 5	24.0 ± 1.7
32.5 ± 7.5	14.4 ± 1.1
50 ± 10	13.6 ± 1.0
70 ± 10	13.1 ± 1.1
90 ± 10	9.8 ± 1.2
150 ± 50	10.94 ± 0.78
250 ± 50	11.2 ± 1.1
350 ± 50	5.62 ± 0.83
450 ± 50	4.25 ± 0.85

several nuclear properties, among them the α+nucleus potential and the level density prescription. The aim of these improvements was to use more recent developments and to provide a firmer physical basis for the model by reducing the reliance on empirical fine-tuning in the hope that the resultant model would be more reliable far off stability where no experimental data exist. Although there is very little α+nucleus data in the astrophysically relevant energy range, recent attempts have been made to use the available data to obtain an improved global α+nucleus potential. For example, a new potential for the $A=140$ region was obtained [31] by fitting data for ^{143}Nd(n,α) [8], ^{147}Sm(n,α) [4], and ^{144}Sm(α,γ) [32] simultaneously using the NON-SMOKER code. Although a fairly good fit to the (n,α) data could be

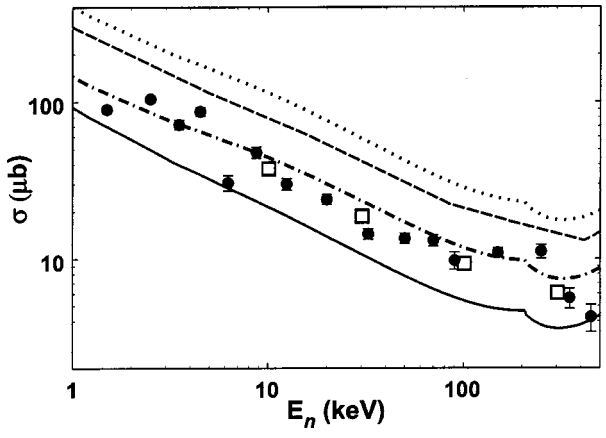

FIG. 3. Measured ^{95}Mo(n,α) cross section averaged over coarse bins (solid circles with error bars) compared to calculations performed with statistical model codes (dashed curve: NON-SMOKER [9]; open squares: Holmes *et al.* [10]; dotted, dot-dashed, and solid curves: MOST [30] using potentials I, II, and III, respectively).

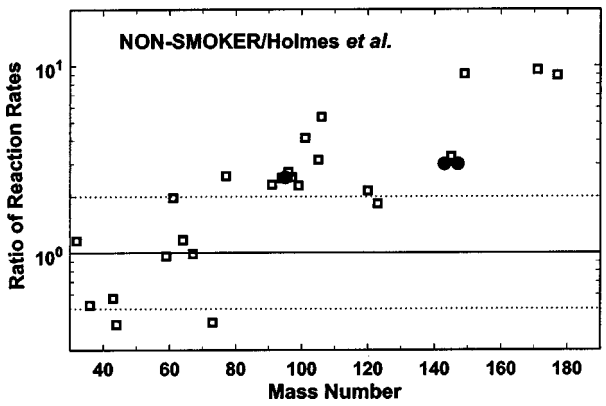

FIG. 4. Ratios of (n,α) reaction rates at $kT=30$ keV calculated with NON-SMOKER [9] to those of Holmes *et al.* [10]. Symbols represent reaction rate ratios for 27 nuclides having calculated cross sections large enough that they should be measurable. Solid circles represent NON-SMOKER/Holmes *et al.* ratios for the three cases (^{95}Mo, ^{143}Nd, and ^{147}Sm) for which measurements have been made. A solid line is drawn at a ratio of unity. Dashed lines at ratios of 0.5 and 2 depict the typical accuracy of (n,γ) reaction rates from global statistical model calculations.

obtained, the ^{144}Sm(α,γ) cross section was overpredicted in the astrophysically relevant range below $E_\alpha=12$ MeV. On the other hand, the same potential yielded good agreement with the measured ^{96}Ru(α,γ) cross section [7], indicating that it may be useful over a more global range. It would be interesting to compare calculations made with this new potential to our new ^{95}Mo(n,α) data.

A wider range of data were fitted in Ref. [30] using the code MOST in an attempt to find a global α+nucleus potential for astrophysical applications, although much of the data was outside the astrophysically interesting range. It was found that three different potentials could describe the data equally well. As can be seen in Fig. 3, the calculation using potential II agrees best with our data and there is about a factor of 5 ratio between the cross sections calculated with potentials I and III. This result is interesting because (α,γ) reaction rates for nuclides involved in the *p* process calculated with the three potentials of Ref. [30] showed some of the largest variations in the mass region near $A=100$, so our new ^{95}Mo(n,α) data should be very useful in the quest to find an improved potential.

The results presented herein for ^{95}Mo(n,α) together with previous (n,α) data for ^{147}Sm [4] and ^{143}Nd [8] are beginning to provide useful constraints for obtaining an improved global α+nucleus potential for nuclear astrophysics. Although there are so far only three data points, it appears that there is better agreement between the data and NON-SMOKER [9] and Holmes *et al.* [10] models as the mass decreases. For example, the ratios of cross sections calculated with NON-SMOKER to the data are 3.3, 2.7, and 2.25 for ^{147}Sm, ^{143}Nd, and ^{95}Mo, respectively, while for the calculations of Holmes *et al.* these ratios are 1.2, 1.0, and 1.0, respectively. As noted previously [4] and as shown in Fig. 4, there is a similar trend with mass between the NON-SMOKER and Holmes *et al.* predictions for (n,α) reaction rates in that the two models are in better agreement with each other at the lower masses. To

obtain the global improvement in the α+nucleus potential needed for *p*-process applications, it will be very important to study these trends on the basis of further experimental data.

ACKNOWLEDGMENTS

We would like to thank K. H. Guber, T. E. Valentine, R. O. Sayer, L. C. Leal, and D. L. Garner for attending the ORELA accelerator during parts of the experiment, V. M. Cauley and T. A. Lewis for keeping ORELA running, and Yu. M. Gledenov for the use of his compensated ion chamber. We would also like to thank S. Goriely for supplying us with the latest cross-section calculations from the statistical model code MOST, and W. Rapp would like to thank the Joint Institute for Heavy Ion Research at Oak Ridge National Laboratory for partial support during the experiments at ORELA. This research was supported in part by the U.S. Department of Energy under Contract No. DE-AC05-00OR22725 with UT-Battelle, LLC.

[1] C. Rolfs and W. S. Rodney, *Cauldrons in the Cosmos* (University of Chicago Press, Chicago, 1988).
[2] S. E. Woosley and W. M. Howard, Astrophys. J., Suppl. **36**, 285 (1978).
[3] M. Rayet, M. Arnould, M. Hashimoto, N. Prantzos, and K. Nomoto, Astron. Astrophys. **298**, 517 (1995).
[4] Yu. M. Gledenov, P. E. Koehler, J. Andrzejewski, K. H. Guber, and T. Rauscher, Phys. Rev. C **62**, 042801R (2000).
[5] P. Mohr, T. Rauscher, H. Oberhummer, Z. Mate, Z. Fülöp, E. Somorjai, M. Jaeger, and G. Staudt, Phys. Rev. C **55**, 1523 (1997).
[6] R. D. Hoffman, S. E. Woosley, T. A. Weaver, T. Rauscher, and F-K. Thielemann, Astrophys. J. **521**, 735 (1999).
[7] W. Rapp, M. Heil, D. Hentschel, F. Käppeler, R. Reifarth, H. J. Brede, H. Klein, and T. Rauscher, Phys. Rev. C **66**, 015803 (2002).
[8] P. E. Koehler, Yu. M. Gledenov, J. Andrzejewski, K. H. Guber, S. Raman, and T. Rauscher, Nucl. Phys. **A688**, 86c (2001); P. E. Koehler, http://www.phy.ornl.gov/astrophysics/nuc/neutrons/whitepaper.pdf
[9] T. Rauscher and F.-K. Thielemann, in *Stellar Evolution, Stellar Explosions, and Galactic Chemical Evolution*, edited by A. Mezzacappa (Institute of Physics, Bristol, 1998), p. 519; T. Rauscher (2001) http://quasar.physik.uinbas.ch/tommy/nosmo.html
[10] J. A. Holmes, S. E. Woosley, W. A. Fowler, and B. A. Zimmerman, At. Data Nucl. Data Tables **18**, 305 (1976).
[11] S. Goriely, in *Nuclei in the Cosmos*, edited by N. Prantzos and S. Harissopulos (Editions Frontieres, Gif-sur Yvette, 1998), p. 314.
[12] A. Antonov, N. Balabanov, Yu. M. Gledenov, Pak Hong Choi, and Yu. P. Popov, Yad. Fiz. **27**, 18 (1978) [Sov. J. Nucl. Phys. **27**, 9 (1978)].
[13] P. E. Koehler, J. H. Harvey, and N. W. Hill, Nucl. Instrum. Methods Phys. Res. A **361**, 270 (1995).
[14] D. H. Wilkinson, *Ionisation Chambers and Counters* (Cambridge University Press, Cambridge, England, 1950), p. 31.
[15] A. Preisart, F. Sauli, Drift and Diffusion of Electrons in Gases: A Compilation, CERN European Organisation of Nuclear Research 84-08 (1984), Figs. 32, 36, and 41.
[16] J. F. Ziegler and J. B. Biersack, SRIM 2000, http://www.reasearch.ibm.com/ionbeams/SRIM/SRIMA.HTM
[17] D. H. Wilkinson, *Ionisation Chambers and Counters* (Cambridge University Press, Cambridge, England, 1950), p. 63.
[18] A. D. Carlson, W. P. Poenitz, G. M. Hale, R. W. Peele, D. C. Dodder, C. Y. Fu, and W. Mannhart, technical report, National Institute of Standards and Technology Report NISTIR-5177, 1993.
[19] N. M. Larson, Technical Report No. ORNL/TM-2000/252, Oak Ridge National Laboratory, 2000.
[20] S. I. Sukhoruchkin, Z. N. Soroko, and V. V. Deriglazov, *Low Energy Neutron Physics* (Springer-Verlag, Berlin, 1998).
[21] S. F. Mughabghab, M. Divadeenam, and N. E. Holden, *Neutron Cross Sections* (Academic, New York, 1981), Vol. 1.
[22] J. A. Harvey, D. J. Hughes, R. S. Carter, and V. E. Pilcher, Phys. Rev. **99**, 10 (1955).
[23] H. E. Jackson, Phys. Rev. **127**, 1687 (1962).
[24] M. I. Pevzner, Yu. V. Adamchuk, L. S. Danelyan, B. V. Efimov, S. S. Moskalev, and G. V. Muradyan, Zh. Eksp. Teor. Fiz. **44**, 1187 (1963).
[25] H. Weigmann and H. Schmid, Nucl. Phys. **A104**, 513 (1967).
[26] S. F. Mughabghab, R. E. Chrien, and O. A. Wasson, Bull. Am. Phys. Soc. **12**, 1199 (1967).
[27] C. Coceva, F. Corvi, P. Giacobbe, and G. Carraro, Nucl. Phys. **A117**, 586 (1968).
[28] H. Shwe and R. E. Cote, Phys. Rev. **179**, 1148 (1969).
[29] H. Weigmann, G. Rohr, and W. Winter, in Proceedings of the Third Conference on Neutron Cross Sections for Technology, Report No. CONF-710301, National Technical Information Service, Springfield, Virginia, 1971, p. 749.
[30] P. Demetriou, C. Grama, and S. Goriely, Nucl. Phys. **A707**, 253 (2002); S. Goriely (private communication).
[31] T. Rauscher, Nucl. Phys. A **79**, 73c (2003); Nucl. Phys. A, in press (Erratum).
[32] E. Somorjai, Z. Fülöp, Á. Z. Kiss, C. E. Rolfs, H. P. Trautvetter, U. Greife, M. Junker, S. Goriely, M. Arnould, M. Rayet, T. Rauscher, and H. Oberhummer, Astron. Astrophys. **333**, 1112 (1998).